Appl. Phys. A 62, 487–492 (1996)

Applied Physics A Materials Science & Processing



# Scattering mechanisms of charge carriers in transparent conducting oxide films

**D.H. Zhang**[1,*], **H.L. Ma**[2]

[1]Department of Physics, Shandong University, Jinan, Shandong 250100, People's Republic of China
(Fax: + 86-531/8902167)
[2]Institute of Optoelectronic Materials and Devices, Shandong University, Jinan, Shandong 250100, People's Republic of China

Received: 23 October 1995/Accepted: 21 December 1995

**Abstract.** Scattering mechanisms of charge carriers in Transparent Conducting Oxide (TCO) films have been analyzed theoretically. For the degenerate polycrystalline TCO films with relatively large crystallite sizes and high carrier concentrations (higher than $5 \times 10^{18}\,cm^{-3}$), the depletion layers between crystallites are very thin compared to the crystallite sizes, and the grain boundary scattering on electrical carriers makes a small contribution to limit the mobility of the films. Instead of thermionic emission current, a tunneling current dominates the electron transport over grain boundaries. The Petritz model which is based on thermionic emission and extensively quoted in literature should not be applicable. The main scattering mechanisms for the TCO films are ionized impurity scattering in the low-temperature range and lattice vibration scattering in the high-temperature range. The ionized impurity scattering mobility is independent of temperature and the mobility due to thermal lattice vibration scattering is inversely proportional to the temperature. The results obtained from Hall measurements on our ZnO, ITO, $SnO_2$ and $SnO_2$:F films prepared with various methods supports the analysis.

**PACS:** 73.50. – h; 73.50.Bk; 73.61.Ga

Transparent Conducting Oxide (TCO) films such as ZnO, $In_2O_3$ and $SnO_2$ have been extensively studied in recent years, because they exhibit high optical transparency (above 90%) in the visible range of light spectrum combined with high electrical conductivity (more than $10^3\,\Omega^{-1}\,cm^{-1}$) that can be attained by an appropriate control of the non-stoichiometry and doping level. These properties are especially suitable for the applications in the field of optoelectronics, ferroelectric memories, selective coating, etc. To date, many kinds of good-quality transparent conducting oxide films have been prepared [1] and a great amount of scattered data on the conduction properties of the TCO films have been obtained. However, many conclusions on the scattering mechanisms of carrier charges are essentially contradictory. For example, Shanthi [2–5] investigated F- and Sb-doped $SnO_2$ films deposited by spray pyrolysis and concluded that grain boundary scattering was the dominant scattering mechanism limiting the mobility of their films. Pisarkiewcz et al. [6] explained the scattering mechanisms for degenerate thin oxide films in terms of intergrain potential barriers and charged point defects. In contrast, some authors indicated that grain boundary scattering made very small contribution to the resistivity of good-quality films and that the main scattering mechanisms dominating the mobility were ionized impurity scattering in the low-temperature range and thermal lattice vibration scattering in the high-temperature range [7–11]. It seems that a consistent picture for the prevailing electrical conduction mechanisms has not yet been established by now and needs further investigation.

In this paper, we give a systematic analysis for conduction mechanisms of practically applied TCO films. The temperature dependence of Hall mobility obtained from Hall measurements on ZnO, $In_2O_3$ and $SnO_2$ films deposited in various methods support our analysis.

## 1 Experiment

The preparations of the ZnO films and the Sn-doped $In_2O_3$ (ITO) films have been reported previously [12–14]. The ZnO films were prepared on Corning 7059 glass substrates by reactively evaporating metallic zinc in an evaporation system with a low-pressure oxygen environment. A low-energy ion beam assisted the deposition during film preparation [12, 13]. The ITO films were deposited on electrically heated glass substrates by simple reactively evaporating In–Sn alloy (Sn, 10 wt%) in a conventional evaporation system with an oxygen environment [14]. The $SnO_2$ and $SnO_2$:F films were made in

*To whom all correspondence should be addressed

a conveyor furnace with atmosphere pressure. A constant-temperature zone in the middle of the furnace was maintained at the required temperature (300–1200 °C). Glass substrates were loaded by a belt into the furnace for film deposition. High purity $N_2$ was used as the carrier gas, passing to the reaction chamber via the bubbles and thereby carrying vapors of $SnCl_4$. Oxygen and fluorine were introduced into the chamber as reaction gas and dopants. The flow rates of fluorine, oxygen and carrier gas through $SnCl_4$ were measured separately by three flowmeters with needle–valve attachments. The flow rates of nitrogen and oxygen were 1 and 0.5–1 l/min, respectively. Deposition of $SnO_2$ and $SnO_2$:F takes place by the simple reactions

$$SnCl_4 + O_2 \rightarrow SnO_2 + 2Cl_2\uparrow,$$

$$SnCl_4 + O_2 + F_2 \rightarrow SnO_2\text{:F} + 2Cl_2\uparrow.$$

Aluminium electrodes were vacuum deposited onto the films in a planar configuration for Hall effect measurements. The measurements were made in a vacuum system with controlled temperatures. Very low temperature was obtained using a liquid helium cooling system.

## 2 Theoretical analysis

For polycrystalline TCO films, main scattering mechanisms for charge carriers are ionized impurity and neutral impurity scattering, thermal lattice vibration scattering and grain boundary scattering. Owing to the concentration and the scattering cross section of the neutral impurities being much smaller than that of ionized impurities both in undoped and doped oxide films, the neutral impurity scattering can be neglected. The reciprocal mobility of the films can be expressed as

$$\frac{1}{\mu} = \frac{1}{\mu_i} + \frac{1}{\mu_l} + \frac{1}{\mu_g}, \tag{1}$$

where $\mu_i$, $\mu_l$ and $\mu_g$ are mobilities corresponding to ionized impurity, lattice vibration and grain boundary scattering, respectively.

### *2.1 Grain boundary scattering*

Polycrystalline TCO films are composed of crystallites joined together by grain boundaries which are transitional regions between different orientations of neighboring crystallites. Among polycrystalline semiconductors, polysilicon has been the most extensively studied material where the grain boundary effects have been analyzed with charge-trapping model [15, 16] where it is assumed that grain boundaries contain lattice defects-induced trapping states. These states compensate a fraction of charge carriers of ionized, uniformly distributed dopants. This process creates a potential barrier across the depletion region, impeding the carrier motion from one crystallite to another. The influence of the grain boundary scattering becomes very important when the width of the depletion layers becomes commensurate with the grain size of the crystallites. This model has been widely applied to the TCO films in the literature [1, 3–6, 17, 18], where it is assumed that grain boundaries between crystallites tend to contain some oxygen which is chemisorbed on the grain boundaries of crystallites. The chemisorbed oxygen atoms (or molecules) can capture electrons from conduction band and makes the grain boundaries negatively charged [19]. So potential barriers are formed between the crystallites, which would strongly scatter conduction electrons. According to the Petritz model [15], the grain boundary scattering-dependent mobility is

$$\mu_g = AT^{-1/2} \exp[-(eV_B/kT)], \tag{2}$$

where $V_B$ is the potential barrier between the grain boundaries, $A = el/(2\pi m^* k)^{1/2}$ is a constant for a sample, the other symbols have their usual significance. In (2), $\mu_g$ is mainly determined by the potential barrier $V_B$. For high-resistivity oxide films, the grain boundary scattering is the main scattering mechanism and $V_B$ is very high (0.6–1.2 eV) [20, 21]. But for the TCO films, many researchers did not observe the thermally activated mobility. This means that $V_B$ is very small and is not even measurable. $V_B$ given by Belonger et al. [22] was 0.01 eV for CVD deposited Sb doped $SnO_2$ films. Shanthi et al. obtained 0.03 eV of $V_B$ for spray pyrolysis deposited undoped $SnO_2$ [5] and 0.02 eV for as-deposited antimony-doped $SnO_2$ [2]. Some values are even smaller than $kT$ at room temperature.

It should be noted that the value of $V_B$ was obtained based on (2) and the formula was derived based on Maxwell-Boltzmann statistics. All good-quality TCO films are degenerate semiconductors. For a degenerate system, Fermi-Dirac statistics should be applied. With Fermi-Dirac statistics, Bruneaux et al. [17] gave another expression for the above mobility,

$$\mu_g = BT^{-1} \exp\left(-\frac{eV_a}{kT}\right) \tag{3}$$

where $V_a$ represents an activation energy related to the electrobarrier $V_B$ by the expression $V_a - V_B - (E_F - E_c)$ ($E_F - E_c$ is the distance between the Fermi level and the bottom of the conduction band in the neutral region), $B$ is a constant. Highly conducting films are degenerate semiconductors and the Fermi level usually shifts upward into the conduction band and subsequently a Burstein shift [23] appears. The Burstein shift was observed in many TCO films [3, 5, 9, 13, 14, 24, 25]. So $V_a = V_B - (E_F - E_c)$ is even smaller than $V_B$.

Figure 1 gives temperature dependence of the thermionic emission mobility for samples with various $V_a$ obtained from (3). The mobility is no longer thermally activated for samples with small $V_B$ when $T > 200$ K (curve *a*, *b* and *c*). For those samples with larger $V_B$ the mobility exhibits slow increases with increasing temperature.

The thickness of depletion layers at grain boundaries can be calculated using formula.

$$d = \sqrt{\frac{2\varepsilon_0 \varepsilon_r V_B}{qn}}. \tag{4}$$

If we assume $n$ to have the order of $10^{20}/cm^3$, the calculated thickness of the potential barriers are only few angstroms (about an atomic layer thick). For the potential

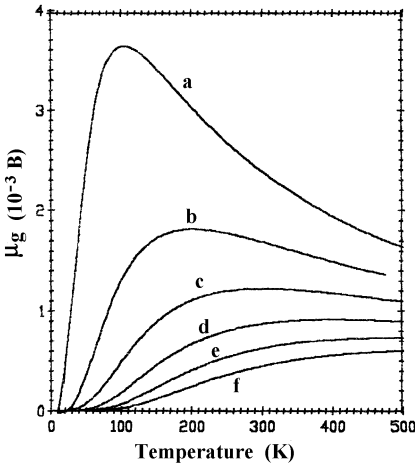


**Fig. 1.** The temperature dependence of thermionic emission mobility. The corresponding $eV_a/k$ for *curve a*, *b*, *c*, *d*, *e*, and *f* are 100 , 200 , 300 , 400 , 500 and 600 K, respectively

barrier with such small thickness, the tunneling current between grains may be dominant, because tunnel probablity [26]

$$T = \exp\left\{ -\frac{2}{\hbar}\int_{x_1}^{x_2} (2m)^{1/2}[U(x) - E]^{1/2}\,\mathrm{d}x \right\}, \tag{5}$$

where $U(x) - E$ is the height of the barriers. For a rectangular barrier with height of $V_a$ and thickness of $d$, the tunnel probability becomes

$$T = \exp\left[ -\frac{2(2meV_a)^{1/2}d}{\hbar} \right]. \tag{6}$$

We can distinguish between thermionic emission and electron tunneling. The electron, as given by Crowell et al. [27], for a current dominated by tunneling, is that the parameter $E_{00}$ is much larger than $kT$. $E_{00}$ is given by

$$E_{00} = 18.5 \times 10^{-12}\left(\frac{n}{m^*\varepsilon}\right)^{1/2} \text{eV}, \tag{7}$$

here $\varepsilon$ is the relative static dielectric constant of the films. For a $SnO_2$ film with $m^* = 0.25\, m_0$, $n = 2.5 \times 10^{20}\ \text{cm}^{-3}$ and $\varepsilon = 10$ [28], the computed $E_{00}$ is equal to 0.181 eV, which is much larger than $kT$ in the temperature range in which the mobility has been measured. So tunneling current makes a major contribution to the transport of electric charges across grain boundaries. Thermionic emission dominates the current only for $n < 5 \times 10^{18}\ \text{cm}^{-3}$ samples. The TCO films with such low carrier concentration cannot be practically applicable.

On another aspect, for good-quality samples with high carrier concentrations and large crystallite sizes, the mean free path of free electrons calculated from $l_e = (h/2e)(3n/\pi)^{1/3}\,\mu$ [8] is only few nm, which is usually much smaller than the crystallite size of the films. This also means that the grain boundary scattering makes a much smaller contribution as compared to other scattering mechanisms and the grain boundary scattering can be ruled out. The grain boundary scattering is dominant to limit the mobility only for those samples whose grain sizes are comparable with mean free path. The samples with such small grain sizes and very low mobility are also not practically useful transparent conducting films.

### *2.2 Ionized impurity scattering*

The TCO films contain a large amount of point defects. These defects are assumed to be oxygen vacancies or/and excess metallic atoms (in undoped films) or external dopants (in doped films). These point defects are usually ionized and become ionized impurities. The concentration of the ionized impurities is larger than $10^{20}\ \text{cm}^{-3}$ for pratically applied films. These ionized impurities are strong scattering centers for charge carriers.

In a degenerate electron system, only the electrons near Fermi level take part in conduction. According to Conwell-Weisskoft formula when degenerate charge carriers are scattered by impurity ions, the energy dependence of mobility is [29]

$$\mu_i = \frac{e}{m^*}\,\tau_i(E_F) = \left(\frac{2}{m^*}\right)^{1/2} \frac{\varepsilon^{1/2}E_F^{3/2}}{\pi e^3 N_i Z^2} \frac{1}{\ln\left(1 + \dfrac{\varepsilon E_F}{N_i^{1/3}Ze^2}\right)^2}, \tag{8}$$

where $\tau_i(E_F)$ is the relaxation time, which takes into account the scattering events occurring near the Fermi level $E_F$, $\varepsilon$ is the static dielectric constant of the films, $m^*$ is the effective mass of electrons, $Ze$ is the ion charge and $N_i$ is the concentration of the scattering centers. Formula (8) does not contain temperature in an explicit way. This means ionized impurity scattering mobility is independent of temperature for the degenerate semiconductors. Shanthi et al. [4], Elich et al. [18] and Huang et al. [8] also obtained an independent temperature dependence for the mobility $\mu_i$ with different approaches.

In contrast with our result, Agnihotry et al. [10] gave a theoretical temperature dependence of the mobility for ionized impurity scattering, $\mu_i \propto T^{3/2}$. This is due to the degeneracy of the investigated material not being taken into account.

### *2.3 Lattice vibration scattering*

As temperature increases, lattice vibration scattering may become dominant. The lattice vibration scattering mobility derived in terms of corpuscular model using deformation potential is [30]

$$\mu_l = \frac{e\pi^2\hbar^4 c_{ll}}{2m^*(2m^*)^{3/2}\Delta_c^2 N}\frac{E^{-1/2}}{kT}, \tag{9}$$

where $c_{ll}$ is elasticity constant modules, $\Delta$ is the divergence of strain, $N$ is the concentration of matrix atoms and other symbols express their usual meaning. Considering the degeneracy for the investigated system, in (9) $E = E_F$ is a constant. So the temperature dependence of the mobility can be written as

$$\mu_l \propto \frac{1}{T}, \tag{10}$$

i.e., the mobility is inversely proportional to $T$.

The temperature dependence of resistivity for a degenerate TCO film can also be expressed by the experimental formula of metal resistivity [17, 28, 31, 32]

$$\rho(T) = \frac{AT^5}{M\Theta_D^6}\int_0^{\Theta_{D/T}} \frac{x^5\,dx}{(e^x - 1)(1 - e^{-x})}, \tag{11}$$

where $T$ is the temperature, $A$ is a characteristic constant for the metal, $M$ is the atomic mass of the metal atom and $\Theta_D$ is the Debye temperature of the metal.

Only at high temperatures, thermal lattice vibration scattering can dominate the mobility of a TCO films. From the above formula, at high temperature, we can get $\rho(T) \propto T$. For degenerate semiconductors, the carrier concentration is independent of temperature. Therefore, the temperature dependence of the mobility can also be written as (10). From another approach, Huang et al. [8] also obtained an inversely proportional temperature dependence for the lattice vibration scattering mobility.

Different from our analysis, based on $E = \frac{3}{2}kT$ in (9), some authors [10, 18, 26] obtained mobility due to lattice vibration dependence as

$$\mu_l = \mu_{0T} T^{-3/2}. \tag{12}$$

Equation (12) was obtained based on Maxwell-Boltzamann statistics. Electrons in the TCO films are degenerate system, Maxwell-Boltzamann statistics is not applicable.

## 3 Experimental results and discussion

The ion-beam-assisted-deposited ZnO films are the degenerately doped $n$-type polycrystalline semiconductor with the hexagonal structure and a preferred orientation with the $c$ axis perpendicular to the substrate. Crystallite sizes average about 25 nm across. The reciprocal temperature dependence of the Hall mobility and the carrier concentration for a typical, transparent conducting film is shown in Fig. 2. In the low temperature range, no significant variation appears both for the Hall mobility and the carrier concentration. However, when temperature is high, a significant increase in $n$ and a marked decrease in $\mu$ occur with increasing temperature.

The ITO films deposited by reactive evaporation are also $n$-type degenerate polycrystalline. The films retained cubic bixbyite structure of the $Mn_2O_3$ (I) type, having lattice parameters corresponding to that of crystal $In_2O_3$. The crystallite sizes estimated from the micrographs are from 60 to 300 nm. The reciprocal temperature dependence of conductivity, carrier concentration and Hall mobility obtained from Hall measurements for a typical film in the temperature range 16–400 K is illustrated in Fig. 3. Both $\mu$ and $\sigma$ remain invariant in the temperature range below 100 K. However, if the temperature is higher than 100 K, they decrease significantly. A similar behavior was observed by Huang et al. in their evaporated ITO films [8].

The APCVD deposited $SnO_2$:F films are also degenerately doped $n$-type semiconductor with carrier concentrations between $3.56 \times 10^{20}/cm^3$ and $7.09 \times 10^{20}/cm^3$, with resistivities in the range from $4.99 \times 10^{-4}$ to $11 \times 10^{-4}\,\Omega cm$ and mobilities from 15.7 to 20.1 $cm^2/v/s$. The films retain the rutile structure with crystallite sizes in the range from 250 to 550 nm. For samples with large crystallite sizes, the surface becomes textured.

The dependence of Hall mobility ($\mu$) and carrier concentration ($n$) on reciprocal temperature for the $SnO_2$:F films at different substrate temperatures, and at different fluorine flow rate is given in Figs. 4 and 5, respectively. As illustrated in Fig. 4, both $n$ and $\mu$ increase with an increase in $T_s$. A similar behavior was reported by Vasu et al. [33]. The increase in $n$ with $T_s$ is due to the enhanced crystallinity and tin atoms present in a tetravalent state [34]. The increase in $\mu$ can be attributed to the improved crystalline nature of the resulting films. It is also observed that for F-doped films, both $\mu$ and $\sigma$ remain constant in the temperature range below 100 K. However, if the temperature is higher than 100 K, a slight increase in $n$ and a significant decrease in $\mu$ occur with an increase in

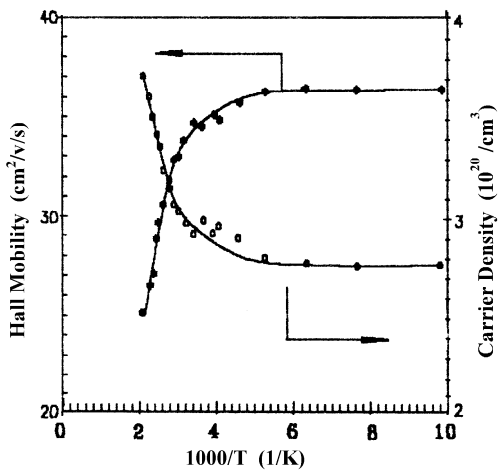


**Fig. 2.** The reciprocal temperature dependence of mobility and carrier concentration of a typical IBAD deposited ZnO films with 90% transmittance and 250 nm thick

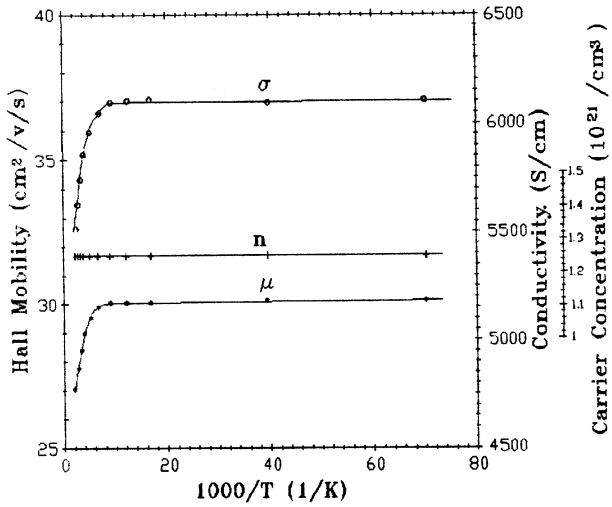


**Fig. 3.** The conductivity, Hall mobility and carrier concentration as a function of $1/T$ ($T$-temperature) for a typical ITO film with 95% transmittance and 125 nm thick

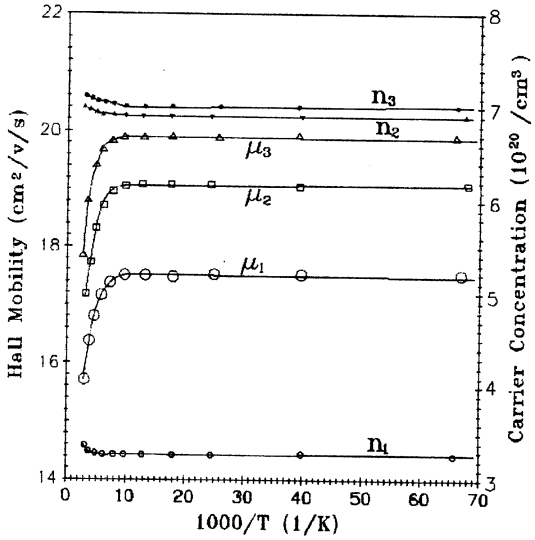


**Fig. 4.** The reciprocal temperature dependence of mobility and carrier concentration of F-doped films deposited at a fluorine flow rate 0.1 l/min and different substrate temperature. For $n_1$, $\mu_1$, $T_s = 400\,^{\circ}C$; $n_2$, $\mu_2$, $T_s = 500\,^{\circ}C$; $n_3$, $\mu_3$, $T_s = 550\,^{\circ}C$

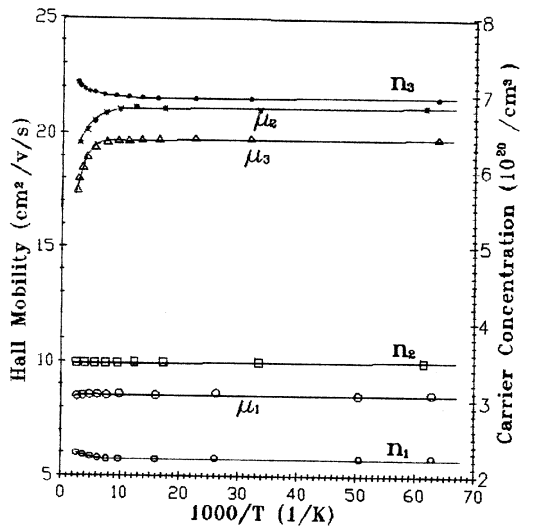


**Fig. 5.** The reciprocal temperature dependence of mobility and carrier concentration of $SnO_2$ films deposited at $T_s = 550\,^{\circ}C$ and different fluorine flow rates. For $n_1$, $\mu_1$, $F = 0$; for $n_2$, $\mu_2$, $F = 0.025$ l/min; for $n_3$, $\mu_3$, $F = 0.1$ l/min

temperature. From Fig. 5, it can be seen that both $n$ and $\mu$ increase markedly with fluorine doping. $n$ shows a gradual increase with an increase in fluorine flow rate, but $\mu$ shows an increase for small fluorine flow rate and then a decrease for large fluorine flow rate. The same characteristic was observed by Shanthi et al. [3]. For undoped samples, both $n$ and $\mu$ remain invariant in the whole investigated temperature range, the invariance in $n$ indicates that the impurity band formed at the shallow donor level has merged with the conduction band [5].

The fluorine flow rate dependence of $\mu$ can be explained as follows. For non-stoichiometric undoped $SnO_2$ films, the doping is assumed to be tin interstitials and/or oxygen vacancies (oxygen vacancies are dominant). These oxygen vacancies are strongly scattering centers which reduce the mobility of $SnO_2$ films significantly (for crystalline $SnO_2$, $\mu = 90\ cm^2/v/s$, but for our undoped $SnO_2$ films, $\mu = 8.5\ cm^2/v/s$). For F-doped $SnO_2$ films, as shallow level $n$-type dopants, F atoms are incorporated in the samples substitutionally that create more free electrons and cause the samples to become more conductive. Waal et al. [35] suggested that in the doping process some involved F atoms may be filled in the oxygen vacancies, this effect would lower the concentration of scattering centers and, hence, increase the mobility of F-doped films. However, when the F content was more than that of the limit needed to fill the oxygen vacancies, the excess ionized F atoms as scattering centers would reduce the mobility of the films.

The temperature dependence of carrier concentration and Hall mobility for the above three kinds of films exhibits a similar characteristic. In the low-temperature range both the carrier concentration and Hall mobility remain invariant. When temperature is high, an increase in the carrier concentration and a decrease in the Hall mobility are observed. The variation of the mobility exhibits an approximately linear decrease with a decrease in $1/T$. The thermal activated mobility was not observed. The increase in $n$ with temperature is attributed to thermal excitation of free electrons of dopants and bulk atoms and the decrease in $\mu$ is due to thermal lattice vibration scattering. The temperature dependence of the Hall mobility in our investigated films coincides with the results of theoretical analysis.

## 4 Conclusion

The theoretical analysis of the scattering mechanisms in the TCO films show that for the degenerate polycrystalline films with large crystallite size (much larger than mean free path of carriers) and high carrier concentration ($n > 5 \times 10^{18}\ cm^{-3}$), in the low-temperature range, ionized impurity scattering dominates the Hall mobility of the films and the Hall mobility is independent of temperature, in the high-temperature range thermal lattice vibration becomes a major scattering mechanism and the mobility is inversely proportional to temperature. The tunnel current is a main transport path at grain boundaries, which is independent of temperature. The grain boundary scattering plays a major role only in the TCO films with small crystallite size and/or low carrier concentration. Hall mobility measurements in our ion beam assisted deposited ZnO films, reactive evaporation prepared ITO films and APCVD made $SnO_2$ : F films identify the above analysis.

*Acknowledgement*. This work was supported by National Education Committee of China.

## References

1. K.L. Chopra, S. Major, D.K. Pandya: Thin Solid Films **102**, 1 (1983)
2. E. Shanthi, A. Banerjee, V. Dutta, K.L. Chopra: Thin Solid Films **71**, 237 (1980)

3. E. Shanthi, A. Banerjee, K.L. Chopra: Thin Solid Films, **88**, 93 (1982)
4. E. Shanthi, A. Banerjee, V. Dutta, K.L. Chopra: J. Appl. Phys. **53**, 1615 (1982)
5. E. Shanthi, V. Dutta, A. Banerjee, K.L. Chopra: J. Appl. Phys. **51**, 6243 (1980)
6. T. Pisarkiewicz, K. Zakrzewska, E. Leja: Thin Solid Films **174**, 217 (1989)
7. G. Sanon, R. Rup, A. Mansingh: Thin Solid Films **190**, 287 (1990)
8. K.F. Huang, T.M. Uen, Y.S. Gou, C.R. Hiang, L.C. Yang: Thin Solid Films **148**, 7 (1987)
9. S. Noguchi, H. Sakata: J. Phys. D **13**, 1129 (1980)
10. S.A. Agnihotry, K.K. Saili, T.K. Saxena, K.C. Nagpal, S. Chandra: J. Phys. D **18**, 2087 (1985)
11. A.K. Saxena, S.P. Singii, R. Thangaraj, O.P. Agnihotri: Thin Solid Films **117**, 95 (1984)
12. D.H. Zhang, D.E. Brodie: Thin Solid Films **213**, 109 (1992)
13. D.H. Zhang, D.E. Brodie: Thin Solid Films **238**, 95 (1994)
14. H.L. Ma, D.H. Zhang, S.Z. Win, S.Y. Li: Thin Solid Films **263**, 105 (1995)
15. R.L. Petritz: Phys. Rev. **104**, 1508 (1956)
16. J.Y.W. Seto: J. Appl. Phys. **46**, 5247 (1975)
17. J. Bruneaux, H. Cachet, M. Froment, A. Messad: Thin Solid Films **197**, 129 (1991)
18. J.J. PH Elich, E.C. Boslooper, H. Haitjema: Thin Solid Films **177**, 17 (1989)
19. D.H. Zhang: J. Phys. D **28**, 1273 (1995)
20. T.L. Tansley, D.F. Neely, C.P. Foley: Thin Solid Films **117**, 19 (1984)
21. T.L. Tansley, D.F. Neely: Thin Solid Films **121**, 95 (1984)
22. D. Belonger, J.P. Dodelet, B.A. Lombos, J.I. Dickson: J. Electrochem. Soc. Solid Sci. Technol. **132**, 1398 (1985)
23. E. Burstein: Phys. Rev. **93**, 632 (1954)
24. E. Mollow: In Proc. Photoconductivity Conf. ed. by R.G. Brecknrige, R.G. Breckenridge, B.R. Russell, E.E. Hahn (Wiley, New York 1954) p. 509
25. B.E. Sernelius, K.-F. Berggren, Z.-C. Jin, I. Hamberg, C.G. Granqvist: Phys. Rev. B **37**, 10244 (1988)
26. R.A. Smith: *Wave Mechanics of Crystalline Solids* (Chapman and Hall,London 1961) p 49
27. C.R. Crowell, V.L. Rideout: Solid-State Electron **12**, 89 (1969)
28. H.J. van Daal: J. Appl. Phys. **39**, 4467 (1968)
29. P.S. Kireev: *Semiconductor Physics* (Mir, Moscow 1978) p. 397
30. Ref [29] p. 442
31. E. Grüneisen: Ann. Phys. (5) **16**, 530 (1933)
F. Bloch: Z. Phys. **59**, 208 (1930)
32. A.N. Gerritsen: *Metalic Conductivity*, *Handbuch der Physik*, Band XIX (Springer, Berlin, Heidelberg (1956) p. 137
33. V. Vasu, A. Subrahmanyam: Thin Solid Films **189**, 217 (1990)
34. M. Tantini, I. Torriani: Thin Solid Films **138**, 255 (1986)
35. H. De Waal, F. Simonis: Thin Solid Films **77**, 253 (1981)